analytical chemistry

pubs.acs.org/ac Article

Chemosensor with Ultra-High Fluorescence Enhancement for Assisting in Diagnosis and Resection of Ovarian Cancer

Lanlan Xu, Hongyu Chu, Dejiang Gao, Qiong Wu, Ying Sun, Zhenxin Wang, Pinyi Ma,* and Daqian Song*

Cite This: *Anal. Chem.* 2023, 95, 2949−2957 Read Online

ACCESS | Metrics & More | Article Recommendations | Supporting Information

ABSTRACT: Fluorescence imaging-guided diagnostics is one of the most promising approaches for facile detection of tumors *in situ* owing to its simple operation and non-invasiveness. As a crucial biomarker for primary ovarian cancers, *β*-galactosidase (*β*-gal) has been demonstrated to be the significant molecular target for visualization of ovarian tumors. Herein, a membrane-permeable fluorescent chemosensor (namely, LAN-*β*gal) was synthesized for *β*-gal-specific detection using the D-galactose residue as a specific recognition unit and LAN-OH (Φ_F = 0.47) as a fluorophore. After *β*-gal was digested, the fluorescence of the initially quenched LAN-*β*gal (Φ_F < 0.001) was enhanced by up to more than 2000-fold, which exceeded the fluorescence enhancement of other previously reported probes. We also demonstrated that the chemosensor LAN-*β*gal could visualize endogenous *β*-gal and distinguish ovarian cancer cells from normal ovarian cells. Further, the chemosensor LAN-*β*gal was successfully applied to visualize the back tumor-bearing mouse model and peritoneal metastatic ovarian cancer model *in vivo*. More importantly, through *in situ* spraying, the proposed chemosensor was successfully employed to assist in the surgical resection of ovarian cancer tumors due to its high tumor-to-normal (T/N) tissue fluorescence ratio of 218. To the best of our knowledge, this is the highest T/N tissue fluorescence ratio ever reported. We believe that the LAN-*β*gal chemosensor can be utilized as a new tool for the clinical diagnosis and treatment of ovarian cancer.

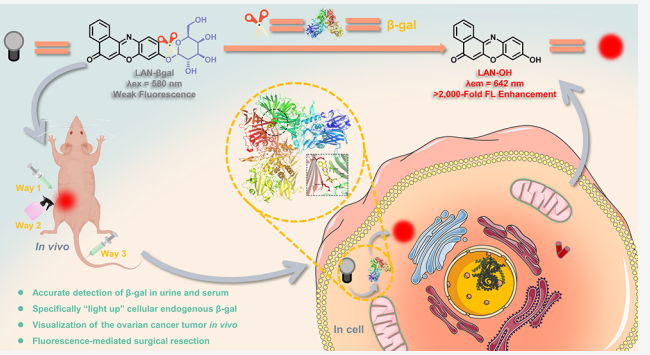

INTRODUCTION

The treatment of malignant tumors has always been a hot topic in biomedical research. At present, surgery is still the main method for the treatment of tumors and is the first choice for early stage tumors.[1−3] In surgical resection of tumors, accurately distinguishing between normal tissues and malignant tumors is of great importance because incomplete resection of tumor lesions can lead to tumor recurrence and excessive resection can usually cause irreversible damage to the body.[4] Conventional tumor diagnosis methods including magnetic resonance (MR),[5,6] ultrasound (US),[7,8] and X-ray computed tomography (CT)[9−11] are limited by their poor capacity in distinguishing between small tumor tissues and normal tissues during clinical surgery.[12] By contrast, fluorescence imaging techniques allow the monitoring of many physiological and pathological processes in real time at the cellular or even at the molecular level.[13−24] In particular, activatable fluorescent probes can be used to potentially guide surgery in real time as they can visualize the location of tumor lesions that are difficult or impossible to detect by human eyes.[25] Thus, a specific, activatable, highly responsive fluorescent probe with a high tumor-to-normal (T/N) tissue fluorescence ratio can be a useful tool for guiding surgical resection of tumors.

β-galactosidase (*β*-gal), an enzyme encoded by the LacZ gene, is a typical glycoside hydrolytic enzyme that can catalyze the hydrolysis of many substrates including ganglioside GM1, lactose, and various glycoproteins.[26] *β*-gal also plays a critical role in cell senescence and is closely associated with various diseases such as *β*-galactosialidosis, Morquio B syndrome, and ovarian cancer.[27−30] Particularly, *β*-gal is one of the primary biomarkers of ovarian cancer, which is the most common gynecological malignancy found worldwide and is responsible for hundreds of thousands of deaths each year.[31,32] Multiple fluorescent probes have been employed in qualitative and quantitative analyses of *β*-gal in evaluating tumor progression, guiding treatment, and predicting prognosis.[27,33−40] Although some of these probes have a relatively large emission

Received: October 25, 2022
Accepted: January 16, 2023
Published: January 25, 2023

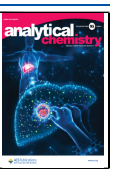

https://doi.org/10.1021/acs.analchem.2c04705
Anal. Chem. 2023, 95, 2949−2957

Scheme 1. Synthetic Route of LAN-βgal

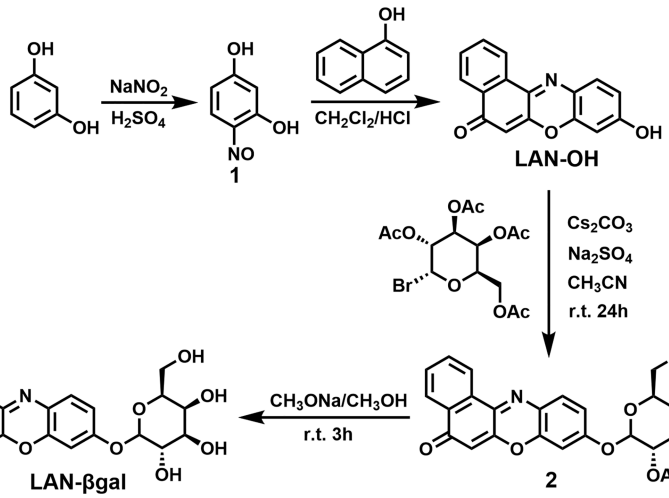

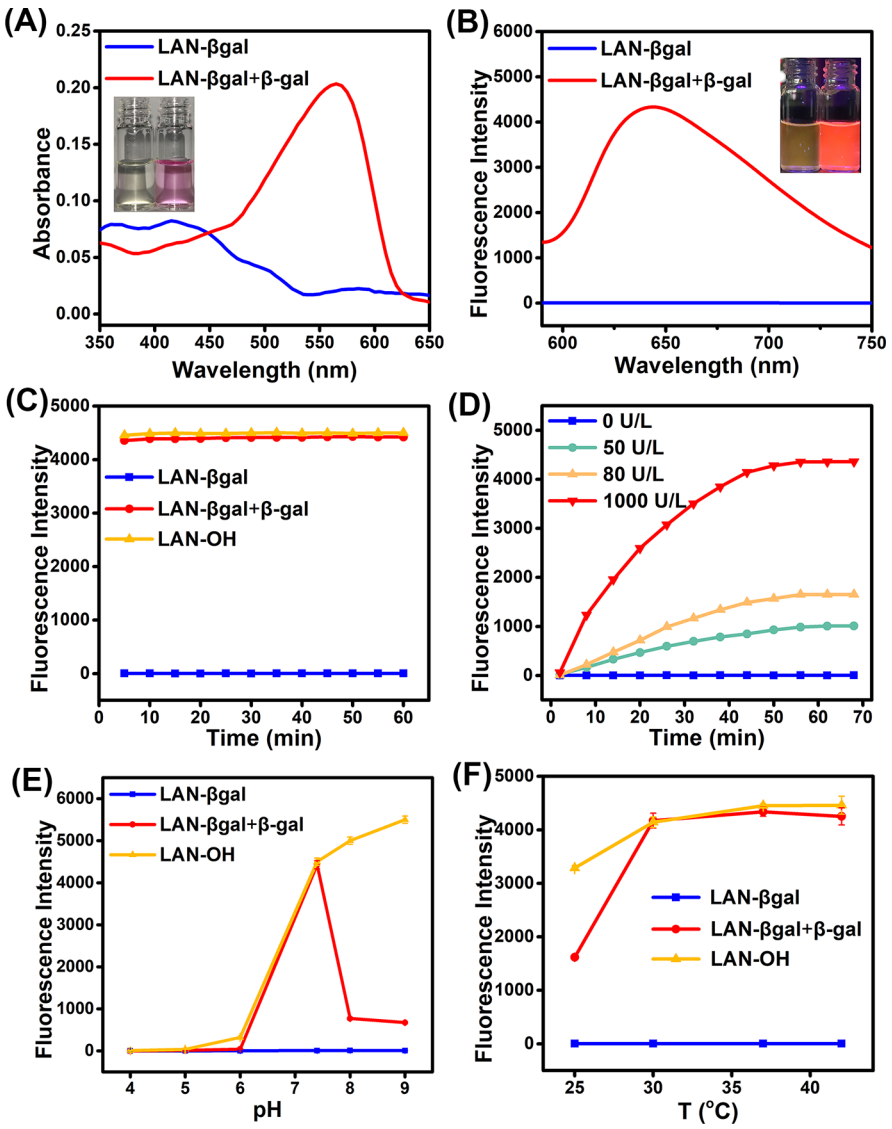

Figure 1. (A) Absorption spectra, (B) fluorescence spectra, and (C) photostability of 10 μM LAN-βgal in the presence or absence of 1000 U/L β-gal in PBS (10 mM, pH 7.4, containing 1% DMSO). (D) Time-dependent fluorescence intensity (λ_{em}max = 642 nm) of 10 μM LAN-βgal incubated with 0, 50, 80, or 1000 U/L β-gal. (E) pH-dependent fluorescence intensity (λ_{em}max = 642 nm) of 10 μM LAN-βgal in the presence or absence of 1000 U/L β-gal. (F) Variation of fluorescence intensities as a function of temperature.

https://doi.org/10.1021/acs.analchem.2c04705
Anal. Chem. 2023, 95, 2949−2957

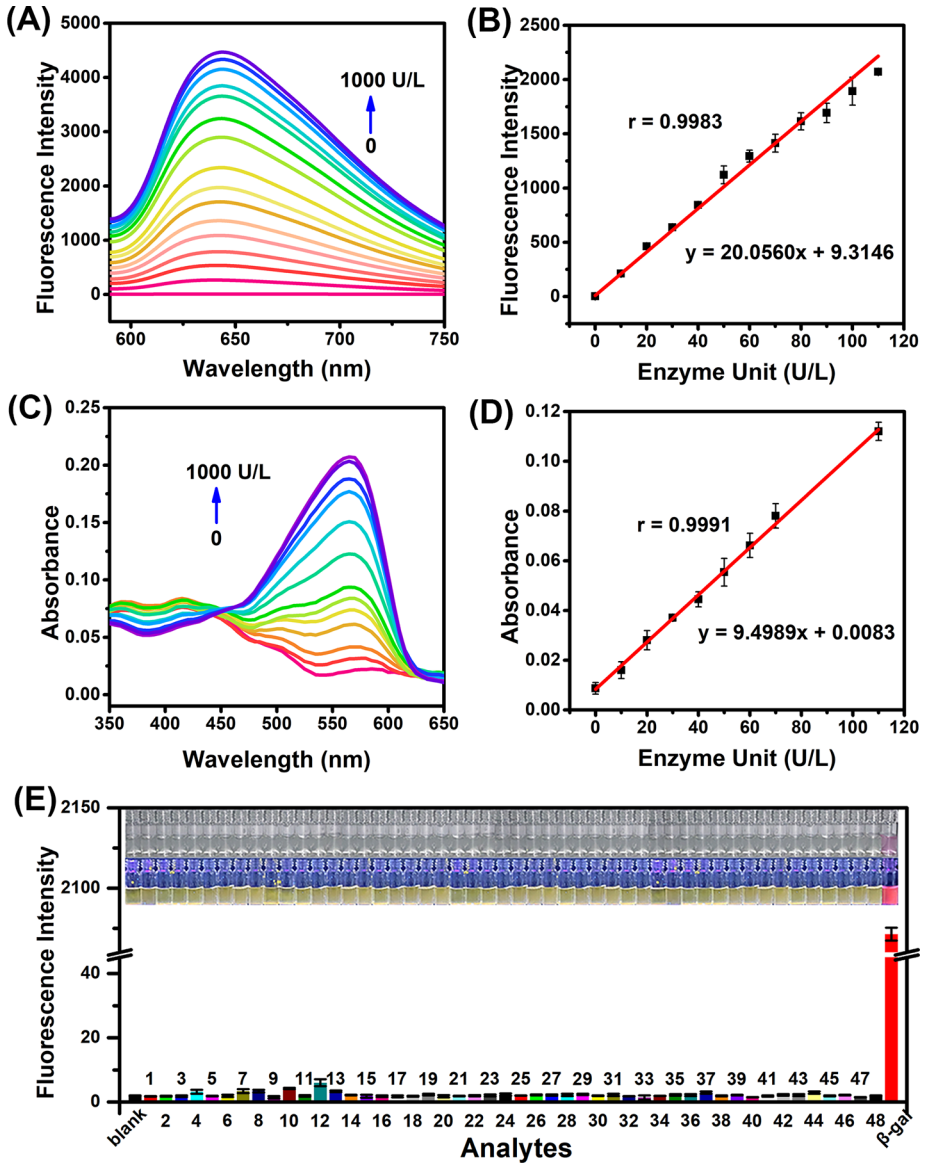

Figure 2. (A) Fluorescence spectra of LAN-βgal (10 μM) in the presence of β-gal at various concentrations (0−1000 U/L). (B) Linear relationship between fluorescence intensity (λ_{em}max = 642 nm) and β-gal concentration (0−110 U/L). (C) Absorption spectra of LAN-βgal (10 μM) in the presence of β-gal at various concentrations (0−1000 U/L). (D) Linear relationship between absorbance at 575 nm and β-gal concentration (0−110 U/L). (E) Fluorescence intensity (λ_{em}max = 642 nm) of LAN-βgal (10 μM) in the presence of various analytes (1 mM unless otherwise stated): 1. Na^+; 2. K^+; 3. Co^{2+}; 4. Fe^{3+}; 5. Ba^{2+}; 6. Li^+; 7. Cu^{2+}; 8. Ag^+; 9. Zn^{2+}; 10. Hg^{2+}; 11. Ca^{2+}; 12. Ni^{2+}; 13. Mg^{2+}; 14. Mn^{2+}; 15. $H_2PO_4^-$; 16. F^-; 17. AcO^-; 18. SO_4^{2-}; 19. Br^-; 20. I^-; 21. CN^-; 22. ClO_4^{2-}; 23. Cl^-; 24. L-Arginine; 25. L-Alanine; 26. DL-Homocysteine; 27. DL-Phenylalanine; 28. L-Cysteine; 29. L-Leucine; 30. DL-Methionine; 31. Glycine; 32. L-Glutamic; 33. D-(+)-Mannose; 34. D-Fructose; 35. Dithiothreitol; 36. L-Ascorbic; 37. Chitosan; 38. H_2O_2; 39. β-Glucuronidase; 40. 1000 U/L aminopeptidase N; 41. 1000 U/L leucine aminopeptidase; 42. 5000 U/L alkaline phosphatase (ALP); 43. 1 μM thrombin; 44. 10 mg/L glucose oxidase; 45. 10 mg/L carcinoembryonic antigen; 46. 10 mg/L albumin bovine V; 47. 20 mg/L hyaluronidase; 48. 7000 U/L maltase.

wavelength (~665 to 725 nm), their fluorescence enhancement is low (~6- to 40-fold) and their fluorescence background is high; as a result, during visualization of β-gal in cells and *in vivo*, their fluorescence changes are not obvious and their T/N tissue fluorescence ratios are low.[15,41−46] Thus far, only a few probes have high fluorescence enhancement. Urano et al. designed a membrane permeability probe, HMREF-βgal, which had a fluorescence enhancement of >1400 times after being activated by β-gal.[47] HMREF-βgal could visualize β-gal activity both *in vitro* and *in vivo* through obvious fluorescence change with a high T/N tissue fluorescence ratio; however, the probe severely suffers from its short emission wavelength (514 nm).

Herein, based on our previous work on the synthesis of fluorophore LAN-OH with high fluorescence quantum yield,[48] we prepared an activatable chemosensor LAN-βgal with intramolecular charge transfer (ICT) characteristic by grafting the D-galactose residue (a specific recognition site) onto LAN-OH (Φ_F = 0.47). The fluorescence intensity of LAN-βgal was quenched (Φ_F < 0.001) upon the addition of the D-galactose residue, resulting in a very low fluorescence background. LAN-βgal was able to ultrasensitively and accurately detect β-gal in urine and serum owing to its high photostability, specificity,

https://doi.org/10.1021/acs.analchem.2c04705
Anal. Chem. 2023, 95, 2949−2957

and sensitivity. LAN-βgal could also specifically "light up" cellular endogenous β-gal and distinguish ovarian cancer cells from normal ovarian cells. Furthermore, the successful fluorescence imaging in both the back tumor-bearing mouse model and peritoneal metastatic ovarian cancer model demonstrated that the chemosensor LAN-βgal could visualize β-gal *in vivo*. More excitingly, through *in situ* spraying, LAN-βgal was successfully used for guiding the surgical resection of ovarian cancer tumors based on its high tumor-to-normal (T/N) tissue fluorescence ratio of 218. Therefore, the proposed chemosensor LAN-βgal has a great potential in clinical diagnosis of ovarian cancer and in *in situ* spraying-based fluorescence imaging-guided surgical resection therapy.

EXPERIMENTAL PROCEDURE

Organic Synthesis. The synthetic route of LAN-βgal is shown in Scheme 1. The reactants and instruments used in the synthesis are shown in the Supporting Information. Compound **1** and LAN-OH were synthesized by previously reported methods[48,49] (see the Supporting Information for the detailed synthesis process of all compounds). The ^{1}H NMR and ^{13}C NMR spectra of LAN-OH were reanalyzed, and the corrected structures are shown in Scheme 1. The ^{1}H NMR, ^{13}C NMR, and LC-HRMS spectra of LAN-OH and LAN-βgal are shown in Figures S1−S6.

Synthesis of Compound **2**. Compound LAN-OH (0.053 g, 0.2 mmol) and 2,3,4,6-tetra-*o*-acetyl-α-D-galactopyranosyl bromide (0.13974 g, 3.4 mmol) were dissolved in 5 mL of acetonitrile. Cs_2CO_3 (0.065 g, 0.2 mmol) and Na_2SO_4 (0.133 g, 0.94 mmol) were then added to the reaction mixture and stirred evenly at room temperature for 24 h. The as-obtained compound **2** was purified by silica gel chromatography using a mixture of methanol and dichloromethane (v/v = 1:200) as the mobile phase. Compound **2** was directly used in the next step without further treatment.

Synthesis of LAN-βgal. Compound **2** (0.1617 g, 0.27 mmol) was dissolved in 4 mL of methanol. Sodium methoxide (0.01325 g, 0.245 mmol) was then added into the solution and stirred evenly at room temperature for 3 h. The as-obtained product was purified by silica gel chromatography using a mixture of methanol and dichloromethane (v/v = 1:100) as the mobile phase. Finally, LAN-βgal (81 mg, 71%), a yellow solid, was obtained. ^{1}H NMR (300 MHz, DMSO-d_6) δ 8.60 (d, J = 6.7 Hz, 1H), 8.13 (dd, J = 7.6, 1.3 Hz, 1H), 7.92−7.77 (m, 3H), 7.18−7.04 (m, 2H), 6.41 (d, J = 4.8 Hz, 1H), 5.31 (d, J = 5.1 Hz, 1H), 5.06 (d, J = 7.6 Hz, 1H), 4.97 (d, J = 5.7 Hz, 1H), 4.74 (t, J = 5.5 Hz, 1H), 4.61 (d, J = 4.7 Hz, 1H), 3.77−3.43 (m, 6H) (Figure S3). ^{13}C NMR (75 MHz, DMSO-d_6) δ 182.56, 160.11, 151.33, 144.94, 144.14, 132.20, 131.43, 131.08, 130.51, 127.57, 125.18, 124.07, 114.44, 106.00, 102.63, 100.69, 75.70, 73.19, 70.08, 68.06, 60.32 (Figure S4). MS (LC-HRMS, m/z) for $C_{22}H_{20}NO_8^+$ [M + H] $^+$: calculated, 426.1183; found: 426.1178 (Figure S6).

Detection of β-Gal in Solution. LAN-βgal was first dissolved in dimethyl sulfoxide (DMSO) to obtain a 1 mM stock solution. The UV−visible spectrum and fluorescence spectrum of LAN-βgal were recorded at 37 °C in 10 mM phosphate buffer solution (PBS, pH 7.4) containing 1% (v/v) DMSO as a co-solvent.

Table 1. Recovery Rates of β-Gal Spiked into Human Urine (n = 3)

sample	β-gal added (U/L)	found by LAN-βgal (U/L)[a]	recovery (%)
blank	0	3.39 ± 0.07	
1	3	6.39 ± 0.05	100.4 ± 0.02
2	6	9.70 ± 0.16	105.3 ± 0.03
3	9	12.67 ± 0.09	103.2 ± 0.01

[a]Mean ± standard deviation.

RESULTS AND DISCUSSION

Characterization of LAN-βgal. In the presence of β-gal, the maximum absorption band of LAN-βgal was shifted from 415 to 575 nm, accompanied with a notable change of color from faint yellow to red (Figure 1A). This is due to the fact that the β-gal-mediated hydrolysis of LAN-βgal released the hydroxyl group as a strong electron donor in the D-π-A structure, which then increased the ICT effect and caused the red shift of the absorption wavelength. LAN-βgal almost had no fluorescence because the ICT effect was weakened by the hydroxyl functionalization of LAN-OH. After reaction with β-gal, the phenolic hydroxyl group on the LAN-OH was liberated, which resulted in the enhancement of the ICT effect, and the fluorescence intensity (λ_{em}max = 642 nm) of LAN-βgal enhanced significantly (Figure 1B). These results demonstrate that LAN-βgal can effectively detect β-gal through both the colorimetric method and fluorescent method. Under continuous irradiation with a 580 nm laser, the change of fluorescence intensities (λ_{em}max = 642 nm) of LAN-βgal before and after reacting with β-gal was negligible (Figure 1C). This result demonstrates that the chemosensor has excellent photostability.

In the presence of β-gal, the fluorescence intensity (λ_{em}max = 642 nm) of LAN-βgal solution increased with increasing reaction time and reached the maximum value within 50 min (Figure 1D). Maximum enhancement of fluorescence intensity (λ_{em}max = 642 nm) was observed at around pH 7.4 (Figure 1E). This may be due to the fact that β-gal has high activity at pH 7.4 but low activity under acidic and alkaline conditions. In addition, the effect of temperatures from 30 to 42 °C on the reaction between LAN-βgal and β-gal was negligible (Figure 1F). Considering that the physiological pH is 7.4, subsequent experiments were carried out at pH 7.4 at 37 °C for 50 min.

Analytical Performance of LAN-βgal. Under the optimal experimental conditions, the fluorescence intensity (λ_{em}max = 642 nm) of LAN-βgal gradually increased with increasing β-gal concentration from 0 to 1000 U/L and reached the maximum value when the β-gal concentration was 1000 U/L (Figure 2A). In particular, the maximum fluorescence intensity of LAN-βgal in the presence of β-gal was more than 2000-fold higher than that in the absence of β-gal (Figure S10). The relationship between the fluorescence signal and β-gal concentration (0−110 U/L) was satisfactorily linear (Figure 2B). The limit of detection (LOD) of the developed chemosensor was calculated (by $3\sigma/k$) to be 0.096 U/L, which is lower than the LOD of other previously reported sensors (Table S1). In addition, the response of LAN-βgal to β-gal at different concentrations was monitored by spectrophotometry. As expected, with the increase in β-gal concentration, the absorbance at 575 nm steadily increased, while that at 415 nm gradually decreased (Figure 2C). A plot of absorbance at 575 nm versus β-gal concentration (0−110 U/L) was linear, and the LOD was calculated (by $3\sigma/k$) to be

https://doi.org/10.1021/acs.analchem.2c04705
Anal. Chem. 2023, 95, 2949−2957

Table 2. Content of β-Gal Detected in Human Urine and Serum (n = 3)

sample	urine 1	urine 2	serum 1	serum 2
found by LAN-βgal (U/L)[a]	3.66 ± 0.06	8.64 ± 0.51	0.41 ± 0.05	0.29 ± 0.03
found by ELISA(U/L)[a]	3.59 ± 0.04	8.47 ± 0.53	0.37 ± 0.11	0.26 ± 0.02

[a]Mean ± standard deviation.

Scheme 2. Molecular Docking Simulation of the Binding between LAN-βgal and β-Gal and HOMO/LUMO Energy Levels of LAN-βgal and LAN-OH

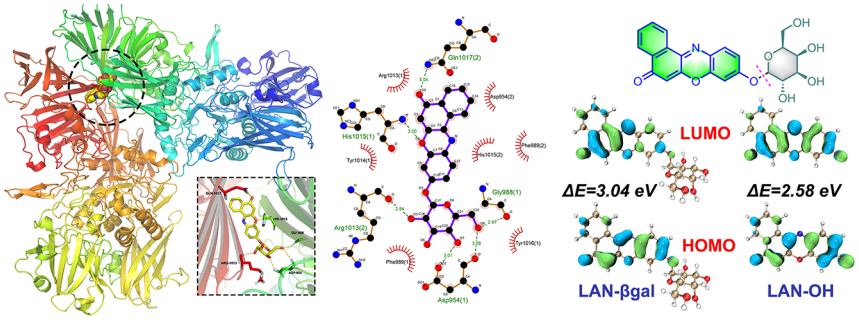

Scheme 3. Proposed β-gal Detection Mechanism of LAN-βgal

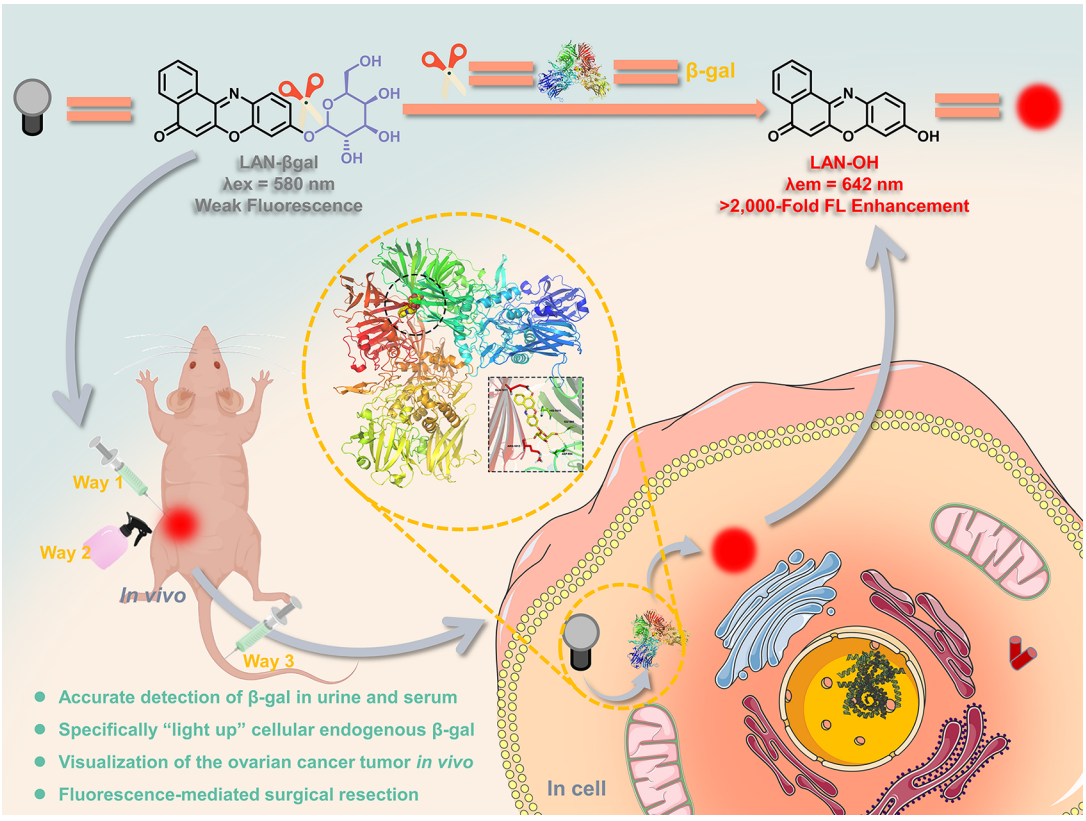

6.9 U/L (Figure 2D). Further, the kinetics of the enzymatic reaction was investigated using the Michaelis−Menten plot and Lineweaver−Burk plot. As shown in Figures S11 and S12, V_{max} = 75.36 μM min^{-1} and K_m = 2.23 μM. The K_m was much lower than that of commercial X-gal (260.6),[41] indicating that LAN-βgal has good affinity for β-gal and is highly sensitive to β-gal.

The selectivity of LAN-βgal for β-gal was evaluated against various potential interfering substances including cations, anions, small molecules, proteins, and enzymes. The response of LAN-βgal to these interfering substances was negligible, demonstrating that LAN-βgal has high selectivity for β-gal (Figure 2E). In addition, we explored the effect of D-galactose (inhibitor of β-gal) on LAN-βgal and LAN-OH (Figure S13). D-Galactose only significantly inhibited the fluorescence intensity of LAN-βgal in the presence of β-gal but had no effect on LAN-βgal and LAN-OH, which further proved that the change of fluorescence intensity originated from the presence of β-gal.

Determination of β-Gal in Human Urine and Serum. First, LAN-βgal was employed to measure the recovery rates of β-gal spiked into human urine samples. As shown in Table 1,

https://doi.org/10.1021/acs.analchem.2c04705
Anal. Chem. 2023, 95, 2949−2957

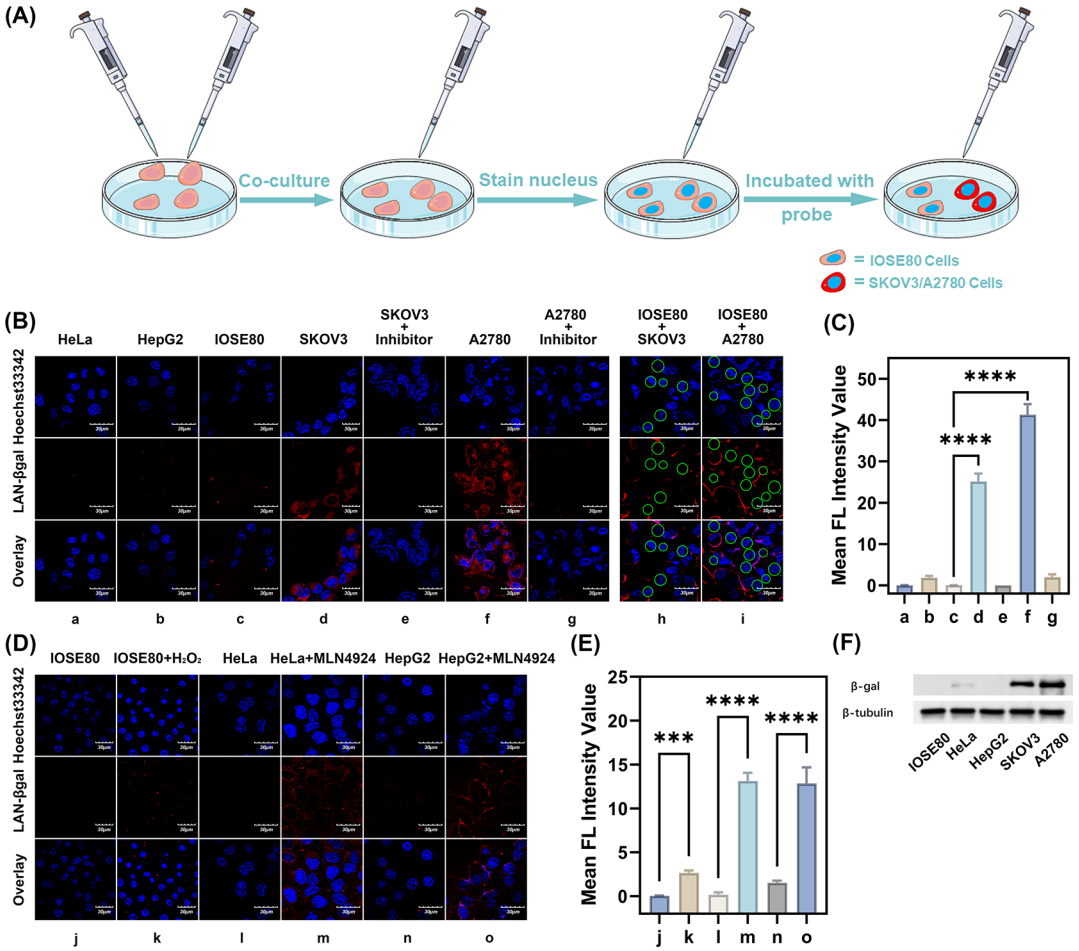

Figure 3. (A) Steps in the cell culture and treatment with the LAN-βgal chemosensor. (B) Fluorescence images of endogenous β-gal in living cells. (C) Mean fluorescence intensity values of cells in panel (B) (****$P < 0.0001$; data analyses were performed on independent samples with equal variances; data are means ± SD; $n = 3$; $\lambda_{ex} = 559$ nm; $\lambda_{em} = 580–680$ nm). (D) Comparison of fluorescence images of non-senescent cells (j, l, and n) and senescent cells (k, m, and o). (E) Mean fluorescence intensity values of cells in panel (D) (****$P < 0.0001$; ***$P < 0.001$; data analyses were performed on independent samples with equal variances; data are means ± SD ($n = 3$); $\lambda_{ex} = 559$ nm; $\lambda_{em} = 580–680$ nm). (F) Western blot analysis of IOSE80, HeLa, HepG2, SKOV3, and A2780 cells (β-tubulin was used as a loading control).

the recovery rates of β-gal in spiked samples ranged from 100.4 to 105.3%, indicating that LAN-βgal can accurately detect β-gal in actual urine samples. Next, LAN-βgal was further employed to measure β-gal in clinical urine and serum samples. As shown in Table 2, the β-gal contents were 3.66 and 8.64 U/L in normal human urine and 0.41 and 0.29 U/L in serum, which were inconsistent with the contents detected by commercial ELISA kits. These results demonstrate that the LAN-βgal chemosensor is a powerful tool for detection of β-gal in a complex biological matrix.

Sensing Mechanism. The sensing mechanism of LAN-βgal toward β-gal was investigated by mass spectrometry, high-performance liquid chromatography (HPLC), molecular docking simulation, and theoretical calculations. In the presence of β-gal, the mass peak of LAN-βgal was shifted from m/z 426.1178 to m/z 264.0656, similarly for the mass peak of LAN-OH (m/z 264.0652) (Figure S7). HPLC analysis of a reaction between LAN-βgal and β-gal showed that a peak for LAN-βgal appeared at 0.99 min, whereas that for LAN-OH appeared at 2.52 min. Peaks for LAN-βgal in the presence of β-gal at a certain concentration appeared at both 0.99 and 2.52 min, each of which was consistent with the peak times of LAN-βgal and LAN-OH, respectively (Figure S14). Molecular docking simulation revealed that LAN-βgal formed six hydrogen bonds with five amino acids (Asp954, Gly988, Arg1013, His1015, and Gln1017) in β-gal. The binding energy for LAN-βgal and β-gal was −10.2 kcal/mol. This result demonstrates that LAN-βgal has a strong binding affinity to β-gal. The molecular orbital of LAN-βgal and LAN-OH was calculated. As shown in Scheme 2, both the highest occupied molecular orbital (HOMO) and lowest unoccupied molecular orbital (LUMO) of LAN-βgal located mainly in the whole fluorophore. Although there was no redistribution of the electronic density on HOMO and LUMO of LAN-OH, the allowed S_1 to S_0 (625.7 nm, $f = 1.1193$) corresponding to a typical ICT led to the strong fluorescence of LAN-βgal after reacting with β-gal. The lower energy gap of LAN-OH (2.58 eV) compared to that of LAN-βgal (3.04 eV) could rationally justify the red shift of absorption wavelengths of LAN-βgal in the absence and presence of β-gal. Based on the above results, we propose that the detection mechanism of LAN-βgal toward β-gal is as follows (Scheme 3): β-gal specifically recognizes and digests the D-galactose unit of LAN-βgal, in turn causing the release of LAN-OH, resulting in the enhancement of fluorescence.

https://doi.org/10.1021/acs.analchem.2c04705
Anal. Chem. 2023, 95, 2949−2957

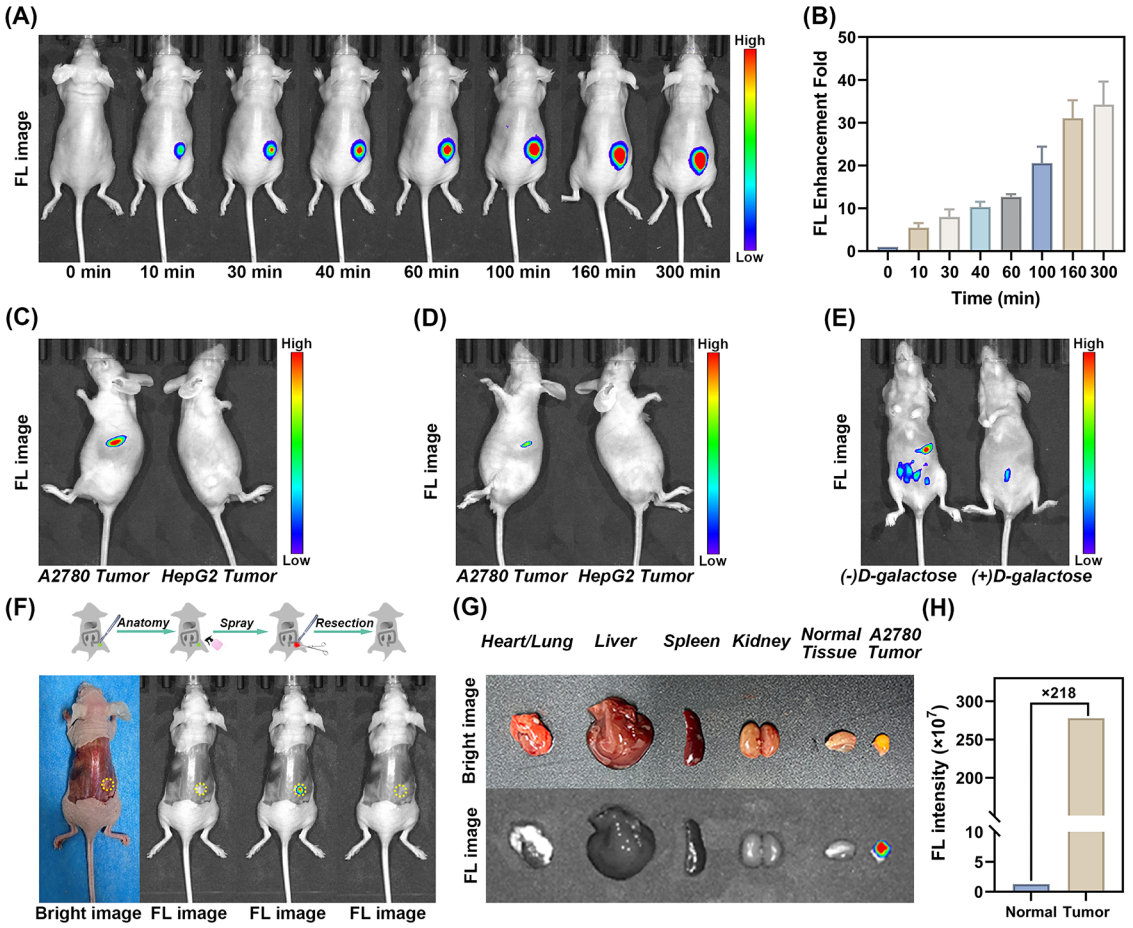

Figure 4. (A) Fluorescence images of β-gal in the A2780 tumor-bearing mouse intratumorally injected with LAN-βgal (200 μM, 50 μL) captured at different times. (B) Change of fluorescence as a function of time at the A2780 tumor site in panel (A). (C) Fluorescence images of β-gal in bare BABL/c mice bearing the A2780 tumor (left) and HepG2 tumor (right) after being intratumorally injected with LAN-βgal (200 μM, 50 μL). (D) Fluorescence images of β-gal in bare BABL/c mice bearing the A2780 tumor (left) and HepG2 tumor (right) after being intravenously injected with LAN-βgal (200 μM, 200 μL). (E) Fluorescence images of β-gal in the peritoneal metastatic tumor model. (F) Imaging-guided resection of the tumor *in situ* spayed with LAN-βgal. (G) Fluorescence images of the main internal organs, normal tissue, and A2780 tumor. (H) Fluorescence intensity of the normal tissue and A2780 tumor.

Visualization of Endogenous β-Gal *In Vitro*. Prior to applying in visualization of β-gal in living cells, the cytotoxicity of LAN-βgal was evaluated by the MTT assay. The viability of cells incubated with LAN-βgal at a concentration as high as 30 μM for 24 h remained higher than 85% (Figure S15), an indication that LAN-βgal has low cytotoxicity. In addition, we evaluated the biocompatibility of LAN-βgal using the hemolysis assay (Figure S16). The hemolysis rate of LAN-βgal at concentrations of up to 200 μM was only 2%, suggesting that it has high biocompatibility. Given its low cytotoxicity and high biocompatibility, LAN-βgal was employed in cell imaging. Five human cell lines were used in this experiment, four of which were human tumor cell lines, including cervical carcinoma (HeLa), liver cancer (HepG2), and two different subtypes of ovarian cancer (SKOV3 and A2780), and one of which was a normal ovarian cell (IOSE80). The fluorescence change of LAN-βgal in A2780 cells with time was investigated (Figure S17). The intracellular fluorescence intensity gradually increased over time until reaching a plateau at 2 h and remained constant for at least 5 h. This indicates that LAN-βgal has high stability during intracellular imaging. In addition, we investigated the cellular localization of LAN-βgal, and the results demonstrated that LAN-βgal localized in the cell membrane (Figure S18). Next, we explored the ability of LAN-βgal in visualizing endogenous β-gal *in vitro*. After routine nuclear staining with Hoechst 33342 for 5 min, cells were incubated with LAN-βgal for 2 h. As shown in Figure 3B, the nuclei of all cells exhibited strong blue fluorescence, and only ovarian cancer cells (SKOV3 and A2780 cells) exhibited a red fluorescence signal. By contrast, the red fluorescence of SKOV3 and A2780 cells pretreated with D-galactose was significantly weakened. These results suggest that the expression level of β-gal in ovarian cancer cells is much higher than that in other types of cells. Interestingly, SKOV3 and A2780 cells (ovarian cancer cells) were found to exhibit a strong red fluorescence signal when they were co-cultured with IOSE80 cells. In addition, we semi-quantitatively assessed the level of β-gal using the western blot (Figure 3F). The content of β-gal was very low in IOSE80, HeLa, and HepG2 cells but very high in SKOV3 and A2780 cells, which is consistent with the results obtained using LAN-βgal. All the above results demonstrate that LAN-βgal can visualize endogenous β-gal and can distinguish ovarian cancer cells from normal ovarian cells.

The relationship between cell senescence and β-gal was further explored using LAN-βgal. As can be clearly observed in Figure 3D, the cells (k, m, and o) pretreated with the cell

https://doi.org/10.1021/acs.analchem.2c04705
Anal. Chem. 2023, 95, 2949−2957

senescence reagent exhibited stronger fluorescence signals than non-senescent cells (j, l, and n). This result suggested that β-gal was closely related to cell senescence, and the expression level of β-gal in senescent cells was much higher than that in non-senescent cells.

Visualization of Endogenous β-Gal *In Vivo*. Inspired by its ability to satisfactorily visualize β-gal *in vitro*, we further employed LAN-βgal to image β-gal *in vivo*. A tumor-bearing mouse was intratumorally injected with LAN-βgal before being subjected to imaging for various times (Figure 4A,B). The results indicated that the fluorescence appeared in the tumor as early as 10 min, and the intensity gradually increased over time until finally reaching a plateau at 160 min. The fluorescence intensity of the tumor remained unchanged for at least 5 h, which is indicative of the high stability of LAN-βgal *in vivo*.

Next, we carried out fluorescence imaging of A2780 tumor- and HepG2 tumor-bearing mice intratumorally injected with LAN-βgal (Figure 4C). As can be clearly seen, the A2780 tumor exhibited strong fluorescence, but the HepG2 tumor did not, which is consistent with the results from *in vitro* experiments. In addition, the results shown in Figure 4D show that the fluorescence of the tumor site of the A2780 tumor-bearing mouse intravenously injected with LAN-βgal was obvious but that of the HepG2 tumor-bearing mouse was not, which is consistent with the observation from intratumoral injection. Finally, we investigated the ability of LAN-βgal to visualize the peritoneal metastatic ovarian cancer tumor. As depicted in Figure 4E, strong fluorescence was observed in the group pretreated with PBS, but weak fluorescence was observed in the group pretreated with D-galactose. This finding further proves that LAN-βgal has high specificity to β-gal. Overall, we demonstrated that the LAN-βgal chemosensor could accurately and specifically detect and visualize β-gal in ovarian cancer mouse models and peritoneal metastatic ovarian cancer models. Therefore, LAN-βgal could be a promising tool for fluorescence imaging-guided diagnosis of ovarian cancer.

***In Situ* Spraying-Based Imaging-Guided Resection.** Owing to its remarkable A2780 tumor imaging ability, LAN-βgal was further used in imaging−guiding surgical resection (Figure 4F). After dissection, the tumor-bearing mouse was subjected to fluorescence imaging. The results showed that the mouse did not exhibit fluorescence signals. By contrast, the tumor site of the mouse evenly sprayed with LAN-βgal on the back exhibited strong fluorescence. After removing the tissue that exhibited fluorescence using a scalpel, the mouse did not exhibit fluorescence, similarly to the control group. This indicates that the tumor tissue was successfully removed. In addition, LAN-βgal could effectively differentiate between the ovarian cancer tissue and normal tissue (Figure 4G) with a T/N tissue fluorescence ratio of 218, which is sufficiently high to allow for accurate identification of cancerous tissues. More importantly, the result further suggests that LAN-βgal could also be used to guide the biopsy of ovarian cancer. Collectively, LAN-βgal can be used as a powerful contrast chemosensor to assist in the surgical resection of ovarian cancer in clinical practice.

CONCLUSIONS

In summary, we developed an enzyme-activatable fluorescent chemosensor LAN-βgal that could monitor endogenous β-gal activity for assisting in surgical resection of ovarian cancer. The transition from the quenched LAN-βgal (Φ_F < 0.001) to LAN-OH (Φ_F = 0.47) led to the fluorescence enhancement by more than 2000-fold. LAN-βgal had high stability and could highly selectively and sensitively detect β-gal in urine and serum samples. In addition, LAN-β-gal was able to specifically "light up" endogenous β-gal and distinguish ovarian cancer cells from normal ovarian cells. Furthermore, the successful fluorescence imaging in tumor-bearing mice demonstrated that LAN-βgal had visualization ability *in vivo*. More importantly, through *in situ* spraying, LAN-βgal was successfully used to assist in the surgical resection of ovarian cancer tumors with a high tumor-to-normal (T/N) tissue fluorescence ratio of 218. Together, the chemosensor LAN-βgal can potentially be applied in clinical diagnosis of ovarian cancer and *in situ* spraying-based fluorescence imaging-guided surgical resection therapy.

ASSOCIATED CONTENT

Supporting Information

The Supporting Information is available free of charge at https://pubs.acs.org/doi/10.1021/acs.analchem.2c04705.

Additional experimental details, including instruments and materials, synthesis, preparation for β-gal detection, determination of the detection limit, determination of fluorescence quantum yield, enzymatic kinetics assays, molecular docking, theoretical calculation and analysis, cell culture, MTT assay, hemolysis assay, establishment of the tumor model, detection of β-gal *in vitro*, detection of β-gal *in vivo*, and supplementary figures and tables (PDF)

AUTHOR INFORMATION

Corresponding Authors

Pinyi Ma − *College of Chemistry, Jilin Province Research Center for Engineering and Technology of Spectral Analytical Instruments, Jilin University, Changchun 130012, China;* orcid.org/0000-0002-3230-4928; Email: mapinyi@jlu.edu.cn

Daqian Song − *College of Chemistry, Jilin Province Research Center for Engineering and Technology of Spectral Analytical Instruments, Jilin University, Changchun 130012, China;* orcid.org/0000-0002-4866-1292; Email: songdq@jlu.edu.cn

Authors

Lanlan Xu − *College of Chemistry, Jilin Province Research Center for Engineering and Technology of Spectral Analytical Instruments, Jilin University, Changchun 130012, China*

Hongyu Chu − *Nanomedicine and Translational Research Center, China-Japan Union Hospital of Jilin University, Changchun 130033, China*

Dejiang Gao − *College of Chemistry, Jilin Province Research Center for Engineering and Technology of Spectral Analytical Instruments, Jilin University, Changchun 130012, China*

Qiong Wu − *Nanomedicine and Translational Research Center, China-Japan Union Hospital of Jilin University, Changchun 130033, China*

Ying Sun − *College of Chemistry, Jilin Province Research Center for Engineering and Technology of Spectral Analytical Instruments, Jilin University, Changchun 130012, China*

Zhenxin Wang − *State Key Laboratory of Electroanalytical Chemistry, Changchun Institute of Applied Chemistry, Chinese Academy of Sciences, Changchun 130022, China;* orcid.org/0000-0002-1908-9848

Complete contact information is available at:

https://doi.org/10.1021/acs.analchem.2c04705
Anal. Chem. 2023, 95, 2949−2957

https://pubs.acs.org/10.1021/acs.analchem.2c04705

Notes

The authors declare no competing financial interest.

■ ACKNOWLEDGMENTS

This work was supported by the National Natural Science Foundation of China (22004046 and 22074052) and the Natural Science Foundation of Jilin Province (YDZJ202101-ZYTS024).

■ REFERENCES

(1) Markhede, G.; Angervall, L.; Stener, B. *Cancer* **1982**, *49*, 1721−1733.
(2) Morgan, W. R.; Zincke, H. *J. Urology* **1990**, *144*, 852−857.
(3) Stephen, M.; Wilson, M. D.; Martin, A.; Adson, M. D. *World J. Gastro. Oncol.* **1976**, *111*, 330−334.
(4) El-Kashlan, H. K.; Zeitoun, H.; Arts, H. A.; Hoff, J. T.; Telian, S. A. *Am. J. Otolaryng* **2000**, *21*, 389−392.
(5) Ma, X.; Tao, H.; Yang, K.; Feng, L.; Cheng, L.; Shi, X.; Li, Y.; Guo, L.; Liu, Z. *Nano Res.* **2012**, *5*, 199−212.
(6) Yang, K.; Hu, L.; Ma, X.; Ye, S.; Cheng, L.; Shi, X.; Li, C.; Li, Y.; Liu, Z. *Adv. Mater.* **2012**, *24*, 1868−1872.
(7) Lee, C. H.; Dershaw, D. D.; Kopans, D.; Evans, P.; Monsees, B.; Monticciolo, D.; Brenner, R. J.; Bassett, L.; Berg, W.; Feig, S.; Hendrick, E.; Mendelson, E.; D'Orsi, C.; Sickles, E.; Burhenne, L. W. *J. Am. Coll. Radiol.* **2010**, *7*, 18−27.
(8) Mallidi, S.; Luke, G. P.; Emelianov, S. *Trends Biotechnol.* **2011**, *29*, 213−221.
(9) Kinsella, J. M.; Jimenez, R. E.; Karmali, P. P.; Rush, A. M.; Kotamraju, V. R.; Gianneschi, N. C.; Ruoslahti, E.; Stupack, D.; Sailor, M. J. *Angew. Chem., Int. Ed.* **2011**, *50*, 12308−12311.
(10) Rabin, O.; Manuel Perez, J.; Grimm, J.; Wojtkiewicz, G.; Weissleder, R. *Nat. Mater.* **2006**, *5*, 118−122.
(11) Wang, H.; Zheng, L.; Peng, C.; Guo, R.; Shen, M.; Shi, X.; Zhang, G. *Biomaterials* **2011**, *32*, 2979−2988.
(12) Li, H.; Yao, Q.; Sun, W.; Shao, K.; Lu, Y.; Chung, J.; Kim, D.; Fan, J.; Long, S.; Du, J.; Li, Y.; Wang, J.; Yoon, J.; Peng, X. *J. Am. Chem. Soc.* **2020**, *142*, 6381−6389.
(13) Chen, Z.; Mu, X.; Han, Z.; Yang, S.; Zhang, C.; Guo, Z.; Bai, Y.; He, W. *J. Am. Chem. Soc.* **2019**, *141*, 17973−17977.
(14) Gu, K.; Liu, Y.; Guo, Z.; Lian, C.; Yan, C.; Shi, P.; Tian, H.; Zhu, W. H. *ACS Appl. Mater. Interfaces* **2016**, *8*, 26622−26629.
(15) Kim, E. J.; Kumar, R.; Sharma, A.; Yoon, B.; Kim, H. M.; Lee, H.; Hong, K. S.; Kim, J. S. *Biomaterials* **2017**, *122*, 83−90.
(16) Lei, Z.; Li, X.; Luo, X.; He, H.; Zheng, J.; Qian, X.; Yang, Y. *Angew. Chem., Int. Ed.* **2017**, *56*, 2979−2983.
(17) Li, H.; Yao, Q.; Xu, F.; Li, Y.; Kim, D.; Chung, J.; Baek, G.; Wu, X.; Hillman, P. F.; Lee, E. Y.; Ge, H.; Fan, J.; Wang, J.; Nam, S. J.; Peng, X.; Yoon, J. *Angew. Chem., Int. Ed.* **2020**, *59*, 10186−10195.
(18) Liu, H. W.; Chen, L.; Xu, C.; Li, Z.; Zhang, H.; Zhang, X. B.; Tan, W. *Chem. Soc. Rev.* **2018**, *47*, 7140−7180.
(19) Murfin, L. C.; Weber, M.; Park, S. J.; Kim, W. T.; Lopez-Alled, C. M.; McMullin, C. L.; Pradaux-Caggiano, F.; Lyall, C. L.; Kociok-Kohn, G.; Wenk, J.; Bull, S. D.; Yoon, J.; Kim, H. M.; James, T. D.; Lewis, S. E. *J. Am. Chem. Soc.* **2019**, *141*, 19389−19396.
(20) Sedgwick, A. C.; Dou, W. T.; Jiao, J. B.; Wu, L.; Williams, G. T.; Jenkins, A. T. A.; Bull, S. D.; Sessler, J. L.; He, X. P.; James, T. D. *J. Am. Chem. Soc.* **2018**, *140*, 14267−14271.
(21) Wu, D.; Sedgwick, A. C.; Gunnlaugsson, T.; Akkaya, E. U.; Yoon, J.; James, T. D. *Chem. Soc. Rev.* **2017**, *46*, 7105−7123.
(22) Yue, Y.; Huo, F.; Ning, P.; Zhang, Y.; Chao, J.; Meng, X.; Yin, C. *J. Am. Chem. Soc.* **2017**, *139*, 3181−3185.
(23) Zhang, J.; Chai, X.; He, X. P.; Kim, H. J.; Yoon, J.; Tian, H. *Chem. Soc. Rev.* **2019**, *48*, 683−722.
(24) Xiong, J.; Wang, Y.; Jiang, X.; Liang, X.; Liang, Q. *Anal. Chem.* **2022**, *94*, 1769−1777.
(25) Zhang, H.; Fan, J.; Wang, J.; Dou, B.; Zhou, F.; Cao, J.; Qu, J.; Cao, Z.; Zhao, W.; Peng, X. *J. Am. Chem. Soc.* **2013**, *135*, 17469−17475.
(26) Juers, D. H.; Matthews, B. W.; Huber, R. E. *Protein Sci.* **2012**, *21*, 1792−1807.
(27) Gao, Y.; Hu, Y.; Liu, Q.; Li, X.; Li, X.; Kim, C. Y.; James, T. D.; Li, J.; Chen, X.; Guo, Y. *Angew. Chem., Int. Ed.* **2021**, *60*, 10756−10765.
(28) Li, X.; Qiu, W.; Li, J.; Chen, X.; Hu, Y.; Gao, Y.; Shi, D.; Li, X.; Lin, H.; Hu, Z.; Dong, G.; Sheng, C.; Jiang, B.; Xia, C.; Kim, C. Y.; Guo, Y.; Li, J. *Chem. Sci.* **2020**, *11*, 7292−7301.
(29) Martinez-Zamudio, R. I.; Dewald, H. K.; Vasilopoulos, T.; Gittens-Williams, L.; Fitzgerald-Bocarsly, P.; Herbig, U. *Aging Cell* **2021**, *20*, No. e13344.
(30) Rouault, C.; Marcelin, G.; Adriouch, S.; Rose, C.; Genser, L.; Ambrosini, M.; Bichet, J. C.; Zhang, Y.; Marquet, F.; Aron-Wisnewsky, J.; Poitou, C.; Andre, S.; Derumeaux, G.; Guerre-Millo, M.; Clement, K. *Diabetologia* **2021**, *64*, 240−254.
(31) Ryan, M.; Williams, C. L.; Galassi, T. V.; Harvey, J. D.; Leicher, R.; Sirenko, M.; Dorso, M. A.; Shah, J.; Olvera, N.; Dao, F.; Levine, D. A.; Heller, D. A. *Sci. Adv.* **2018**, *4*, 1090.
(32) Kim, M.; Chen, C.; Wang, P.; Mulvey, J. J.; Yang, Y.; Wun, C.; Antman-Passig, M.; Luo, H.-B.; Cho, S.; Long-Roche, K.; Ramanathan, L. V.; Jagota, A.; Zheng, M.; Wang, Y.; Heller, D. A. *Nat. Biomed. Eng.* **2022**, *6*, 267−275.
(33) Chen, M.; Mu, L.; Cao, X.; She, G.; Shi, W. *Chinese J. Chem.* **2019**, *37*, 330−336.
(34) Doura, T.; Kamiya, M.; Obata, F.; Yamaguchi, Y.; Hiyama, T. Y.; Matsuda, T.; Fukamizu, A.; Noda, M.; Miura, M.; Urano, Y. *Angew. Chem., Int. Ed.* **2016**, *55*, 9620−9624.
(35) Ito, H.; Kawamata, Y.; Kamiya, M.; Tsuda-Sakurai, K.; Tanaka, S.; Ueno, T.; Komatsu, T.; Hanaoka, K.; Okabe, S.; Miura, M.; Urano, Y. *Angew. Chem., Int. Ed.* **2018**, *57*, 15702−15706.
(36) Kim, E.-J.; Podder, A.; Maiti, M.; Lee, J. M.; Chung, B. G.; Bhuniya, S. *Sens. Actuat. B Chem.* **2018**, *274*, 194−200.
(37) Li, Z.; Ren, M.; Wang, L.; Dai, L.; Lin, W. *Sens. Actuat. B Chem.* **2020**, *307*, No. 127643.
(38) Sharma, A.; Kim, E. J.; Shi, H.; Lee, J. Y.; Chung, B. G.; Kim, J. S. *Biomaterials* **2018**, *155*, 145−151.
(39) Zhang, X. X.; Wu, H.; Li, P.; Qu, Z. J.; Tan, M. Q.; Han, K. L. *Chem. Commun.* **2016**, *52*, 8283−8286.
(40) Zhu, R.; Wang, S.; Xue, Z.; Han, J.; Han, S. *Chem. Commun.* **2018**, *54*, 11566−11569.
(41) Gu, K.; Xu, Y.; Li, H.; Guo, Z.; Zhu, S.; Zhu, S.; Shi, P.; James, T. D.; Tian, H.; Zhu, W. H. *J. Am. Chem. Soc.* **2016**, *138*, 5334−5340.
(42) Li, X.; Pan, Y.; Chen, H.; Duan, Y.; Zhou, S.; Wu, W.; Wang, S.; Liu, B. *Anal. Chem.* **2020**, *92*, 5772−5779.
(43) Lozano-Torres, B.; Blandez, J. F.; Galiana, I.; Garcia-Fernandez, A.; Alfonso, M.; Marcos, M. D.; Orzaez, M.; Sancenon, F.; Martinez-Manez, R. *Angew. Chem,. Int. Ed.* **2020**, *59*, 15152−15156.
(44) Shi, L.; Yan, C.; Ma, Y.; Wang, T.; Guo, Z.; Zhu, W. H. *Chem. Commun.* **2019**, *55*, 12308−12311.
(45) Zhang, J.; Li, C.; Dutta, C.; Fang, M.; Zhang, S.; Tiwari, A.; Werner, T.; Luo, F. T.; Liu, H. *Anal. Chim. Acta* **2017**, *968*, 97−104.
(46) Zhen, X.; Zhang, J.; Huang, J.; Xie, C.; Miao, Q.; Pu, K. *Angew. Chem., Int. Ed.* **2018**, *57*, 7804−7808.
(47) Asanuma, D.; Sakabe, M.; Kamiya, M.; Yamamoto, K.; Hiratake, J.; Ogawa, M.; Kosaka, N.; Choyke, P. L.; Nagano, T.; Kobayashi, H.; Urano, Y. *Nat. Commun.* **2015**, *6*, 6463.
(48) Xu, L.; Zhang, Y.; Zhao, L.; Han, H.; Zhang, S.; Huang, Y.; Wang, X.; Song, D.; Ma, P.; Ren, P.; Sun, Y. *Talanta* **2021**, *233*, No. 122578.
(49) Xu, L.; Wu, M.; Zhao, L.; Han, H.; Zhang, S.; Ma, P.; Sun, Y.; Wang, X.; Song, D. *Talanta* **2020**, *215*, No. 120892.